Defect physics in intermediate-band materials: Insights from an optimized hybrid functional

Miaomiao Han,[1,2,3] Zhi Zeng,[1,2,*] Thomas Frauenheim,[3] and Peter Deák[3,†]

[1]*Key Laboratory of Materials Physics, Institute of Solid State Physics, Chinese Academy of Sciences, Hefei 230031, China*

[2]*University of Science and Technology of China, Hefei 230026, China*

[3]*Bremen Center for Computational Material Science, University of Bremen, Bremen D-28344, Germany*

(Received 26 July 2017; revised manuscript received 2 October 2017; published 18 October 2017)

Despite the efforts to implement the idea of a deep level impurity intermediate band (IB) into bulk solar cell materials, a breakthrough in efficiency increase has not yet been achieved. Taking Sn-doped $CuGaS_2$ as an example, we investigate the problem here from the perspective of defect physics, considering all possible charge states of the dopant and its interaction with native defects. Using an optimized hybrid functional, we find that Sn_{Ga} has not only a donor-type (+/0), but also an acceptor-type (0/−) charge transition level. We estimate the probability of the optical transition of an electron from/to the neutral defect to/from the conduction-band edge to be about equal, therefore, the lifetimes of the excited carriers are probably quite short, limiting the enhancement of the photocurrent. In addition, we find that doping with Sn_{Ga} leads to the spontaneous formation of the intrinsic acceptor Cu_{Ga} defects which passivate the donor Sn_{Ga} and pin the Fermi level to a position (1.4 eV above the valence-band edge) where both defects are ionized. As a result, the possibility of absorption in the middle of the visible range gets lost. These two recombination and passivation mechanisms appear to be quite likely the case for other donors and other similar host materials as well, explaining some of the experimental bottlenecks with IB solar cells based on deep level impurities.

DOI: 10.1103/PhysRevB.96.165204

I. INTRODUCTION

Considering the pressing energy demand and the ecological problems of modern society, clean and renewable energy at low cost has become an urgent necessity. Solar cells are one of the possible solutions, and photovoltaic devices with ever increasing efficiency and diminishing cost are a major subject of research and development today. The intermediate band solar cell (IBSC) [1–3] where an additional intermediate band (IB) in the fundamental band gap acts as the stepping stone to absorb two low-energy photons could realize a high conversion efficiency. An ideal IBSC with a single partially filled and isolated IB could reach a theoretical efficiency limit of 40.7% [4], well exceeding the Shockley-Queisser limit for single-junction solar cells (31%) [5]. Therefore, much effort has been devoted to the implementation of the IBSC idea using quantum dots [6–11], highly mismatched alloys [12–16], or bulk semiconductors with a high concentration of deep level impurities [17]. The latter are relatively easy to fabricate, so many different hosts, such as III–V, II–VI, spinel compounds [18], as well as chalcopyrite materials [19–25] have been studied, both experimentally and theoretically with several dopants. $CuGaS_2$, a chalcopyrite crystal related to the CIGS [i.e., $Cu(In,Ga)Se_2$] family of solar cell materials [26,27] has attracted much attention as a potential IB host since it has a relatively wide band gap [28,29] close to the optimal value [4]. Until now at least four elements, Ti, Cr, Fe, and Sn [3,30–34] have been observed experimentally to introduce IBs in the band gap of $CuGaS_2$. In all these cases sub-band gap optical absorption was reported, corresponding to electron transitions from the valence band (VB) to the IB and/or from the IB to the conduction band (CB) [35]. In the case of Ti_{Ga}, an increase in the photocurrent also was observed [30]. However, in the case of Fe_{Ga}, even though the optical absorption has increased with increasing Fe content, current collection and open-circuit voltage have decreased significantly [3]. To our knowledge no photocurrent measurement has been made for Sn_{Ga}, and only an insignificant enhancement was observed in the absorption. In a photoluminescence (PL) study [33] on $CuInS_2$:Sn_{Ga}, only IB-to-VB emission was observed, but no emission from the CB to the IB was observed. The situation is, therefore, quite confusing, while obviously no breakthrough could be reached in terms of efficiency. Theoretical calculations so far only focused on pinpointing appropriate impurities which can introduce an IB into the band gap and enhance the optical absorption [19–25,36]. Defects of $CuGa(In)Se_2$ have, however, been investigated intensively. Earlier work using the local-density approximation (LDA) of density functional theory (DFT) had to rely on *ad hoc* corrections to estimate the position of defect levels [37–39], while more recently, the Heyd-Scuseria-Ernzerhof (HSE) hybrid functional [40,41] has been applied with the screening parameter tuned to reproduce the room-temperature (RT) optical band gap in CIGS materials [42]. To our knowledge, interaction of the dopant with native defects has hardly been considered. Complex formation or competition for given sites in the lattice with and compensation or passivation by the native defects can impair the effect of dopants [43], so this must be investigated.

Here we perform a case study for the donor Sn_{Ga} in $CuGaS_2$. To obtain a reliable description of the defects, we optimize first the screened hybrid functional. The mixing and screening parameters α and μ, respectively, of the HSE hybrid have been tuned to reproduce the band gap and to fulfill the generalized Koopmans' theorem (gKT) in order to provide the total energy as the correct piecewise linear function of the occupation numbers [44,45]. We find that the same parameters can fulfill these criteria both in $CuGaSe_2$ and in $CuGaS_2$. The optimized hybrid is evaluated by comparing to published theoretical

*zzeng@theory.issp.ac.cn

†peter.deak@uni-bremen.de

 ©2017 American Physical Society

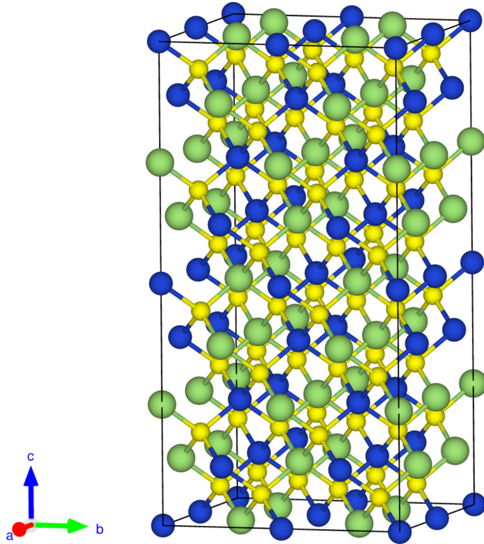

FIG. 1. The 128-atom supercell of $CuGaS_2$. Cu: blue spheres; Ga: green spheres; S: yellow spheres.

results and experimental data. We find good agreement in the structural parameters and the band structure. Since information on the defects is scarce in $CuGaS_2$, we compare to published theoretical results on the charge transition levels of the antisite defects Ga_{Cu} and Cu_{Ga} in $CuGaSe_2$ as well as to experimental data on the PL related to the latter. Applying then the optimized hybrid to study the defects in $CuGaS_2$, we find that Sn_{Ga} is strongly amphoteric, which indicates a short lifetime for the carriers produced by optical excitation. In addition, we will show that the Cu_{Ga} antisite defects can passivate the Sn_{Ga} donors, removing the expected absorption in the midvisible range. The mechanism derived here is of great significance to understand and, to some extent, explain the experimental results in IB solar cells based on deep level impurities. The paper is organized as follows. The general computational framework is introduced in Sec. II A, whereas Secs. II B and II C describe the optimization and tests, respectively, of the hybrid functional. In Sec. III we summarize our results on the Sn_{Ga} and Cu_{Ga} defects in $CuGaS_2$ and discuss the implications on the optical properties. The conclusions are drawn in Sec. IV.

II. METHODS

A. Computational framework

Figure 1 shows the 128-atom perfect $CuGaS_2$ supercell ($2 \times 2 \times 2$ multiple of the body-centered tetragonal conventional cell), which is applied in this paper for defect calculations. The cations are coordinated tetrahedrally by four S atoms, and the anions are surrounded by two Cu atoms and two Ga atoms. Our calculations have been performed within the framework of density functional theory using the Vienna *Ab initio* Simulation Package, VASP 5.3.3 [46–48]. We employ the projector augmented-wave method [49,50] and treat the Ga 3*d* electrons as part of the core since our test has shown that they have a negligible effect on the band gap (0.01 eV). The Cu 3*d* electrons are, of course, treated in the valence shell. A 400- (800-) eV cutoff is applied for the expansion of the wave functions (charge density). The fulfillment of the generalized Koopmans' theorem was achieved for the donor level of the relaxed neutral Sn_{Ga} defect in a 128-atom supercell with experimental lattice parameters [51]. The equilibrium lattice parameters then were determined using the optimized hybrid for the eight-atom unit cell with a $6 \times 6 \times 6$ Monkhorst-Pack (MP) k-point set [52] performing constant volume relaxations and then fitting to Murnaghan's equation of state [53,54]. Defect calculations are all carried out using the equilibrium lattice parameters in the 128-atom supercell with the Γ approximation for Brillouin-zone sampling. Tests with a Γ-centered $2 \times 2 \times 1$ MP set have shown that the single-particle gap levels of Sn_{Ga} in $CuGaS_2$ as well as of Ga_{Cu} and Cu_{Ga} in $CuGaSe_2$ change by less than 0.1 eV at the Γ point. The dispersion of the defect band among the given k points is, however, significant. This affects the total energy by about 0.2 eV, so calculated adiabatic charge transition levels are not fully size converged. Unfortunately, we cannot afford to carry out defect relaxations on a large scale with a $2 \times 2 \times 1$ MP set nor a larger supercell. The force criterion of relaxation was 0.02 eV/Å.

The defect's formation energy is calculated according to the equation [55,56],

$$\Delta E^{i,q}_{\text{form}} = E^q - E_{\text{host}} + \sum_i n_i \mu_i + q(E_V + E_F + \Delta V_{\text{align}}) + E^q_{\text{corr}}, \quad (1)$$

where E^q is the total energy of the supercell with a defect in charge state q, E_{host} is the total energy of the perfect supercell without the defect, n_i is the number of atoms of type i, introduced into the supercell when forming the defect, and μ_i is the chemical potential of that atom in its standard state: in our case metallic Cu, Ga, and Sn. Hybrid functionals do not work well for metals, so our optimized hybrid functional does not treat them on the same footing as the semiconductors investigated here. Therefore, we have calculated the energy of the atoms by the optimized hybrid functional and then deducted the experimental atomization energy [57] to obtain the chemical potential in the metallic state. E_F is the Fermi energy, referenced to E_V, the valence-band maximum (VBM) in the bulk. ΔV_{align} is the potential alignment between the neutral defect and the perfect cell, and E^q_{corr} is the energy correction of the charged defect [58]. Both the total energy and the Kohn-Sham (KS) level of localized states were corrected *a posteriori*. Total energy corrections were obtained by the method of Freysoldt, Neugebauer, and Van de Walle, [59], whereas localized defect levels were corrected using the relation $e^{\text{level}}_{\text{corr}} = -2E^{tot}_{\text{corr}}/q$, derived by Chen and Pasquarello [60]. In the corrections we have used the directional average of the experimental high-frequency dielectric constants $\varepsilon_\infty = 6.17$ for $CuGaS_2$ [61,62] and 7.47 for $CuGaSe_2$ [63], both for vertical (fixed ions) and adiabatic (relaxed ions) charge transitions. In principle, the static dielectric constant ε_0 should be used in the adiabatic case, but experience has shown that applying the bulk value of ε_0 to describe the ionic screening of a charge in a supercell of quite limited size introduces a bigger error than using ε_∞ instead [44]. We provide the raw energy results together with the applied corrections in the Supplemental Material [64].

TABLE I. The band gap of a 128-atom $CuGaS_2$ supercell, and the fulfillment of the generalized Koopmans' theorem in the case of Sn_{Ga} for various HSE(α,μ) functionals. All values are in eV.

α/μ	E_g	ΔKS_{HOMO} (N)	ΔE_{SCF}	ΔKS_{LUMO} $(N-1)$
0.25/0.2 (standard HSE06)	2.12	−1.14	−1.35	−1.55
0.30/0.2 (Ref. [83])	2.38	−1.31	−1.47	−1.62
0.25/0.13 (Ref. [42])	2.32	−1.33	−1.44	−1.53
0.26/0.08 (present paper)	2.55	−1.55	−1.56	−1.57

Assuming thermodynamic equilibrium during growth, the concentration of the defects in their different charge states can be predicted from the calculated formation energies by solving the neutrality equation,

$$N_C \exp\left[-\frac{E_C - E_F}{kT}\right] + \sum_i |q_i|(N_{Ai} - p_{Ai}) = N_V \exp\left[-\frac{E_F - E_V}{kT}\right] + \sum_i |q_i|(N_{Di} - n_{Di}), \quad (2)$$

where N_{Di}, N_{Ai} are the concentrations of the various donor and acceptor defects, respectively, as determined by their formation energy. N_C, N_V are the effective density of states at the conduction-band and the valence-band edges, and n_{Di}, p_{Ai} are the concentration of electrons on donor states and of holes on acceptor states, respectively. Details can be found, e.g., in Ref. [65]. Since the defect concentration itself is dependent on the Fermi level through the formation energy, Eqs. (1) and (2) have to be solved iteratively. To calculate N_C and N_V, the effective masses $m_e^* = 0.12m_0$ and $m_h^* = 0.68m_0$ have been used for electrons and holes, respectively [66,67]. The temperature was set to 1000 K, which is typical in the chemical vapor transport growth of $CuGaS_2$ [68].

B. Optimization of the HSE (α,μ) parameters

The total energy in exact DFT is a piecewise linear function of the occupation numbers of the Kohn-Sham orbitals [69–71]. From the linearity follows the gKT, i.e., the independence of the Kohn-Sham energy levels from their occupation [72] with that of the frontier orbital providing the (vertical) ionization energy [73]. In contrast, the standard local (LDA) and semilocal [generalized gradient approximation (GGA)] exchange approximations suffer from the lack of a derivative discontinuity and from a positive (convex) curvature [74,75]. The former leads to serious underestimation of the band gap and thus to incorrect band-edge positions, whereas the latter leads to an artificial delocalization of the defect states. Defect levels can, therefore, not be accurately predicted in wide band-gap semiconductors. In recent years, hybrid functionals have emerged as a useful alternative [76–78]. The screened hybrid functional HSE [40,41] is a semiempirical mixture of the GGA exchange of Perdew, Burke, and Ernzerhof [79] with a given fraction α of nonlocal Hartree-Fock- (HF-) type exchange, which brings back the derivative discontinuity. To account for screening, the mixing is being phased out by an error function beyond a distance of $2/\mu$, where μ is the screening parameter. In the standard HSE06 version, the mixing parameter $\alpha = 0.25$ and screening parameter $\mu = 0.2$ were found to be optimal, leading to the best band gap for a large number of semiconductors. The screening is critical, and the value chosen in the standard HSE06 works well for semiconductors with medium screening but not so well for ionic insulators [80,81], whereas it breaks down for metals [82]. If HSE06 does not reproduce the gap of a given material, usually either α or μ is tuned [42,83,84] without consideration to the issue of localization of the defect states and the fulfillment of the gKT. Actually, HSE-type hybrids offer a useful opportunity for mimicking the self-interaction-free functional of exact DFT by error compensation. Both the correct band gap and the compliance to the gKT can be achieved by tuning α and μ simultaneously. In other words, our goal is to achieve the correct piecewise linear dependence of the total energy as a function of the occupation numbers. It has been shown earlier that the standard HSE06 fulfills these criteria for group-IV semiconductors [85,86] and for TiO_2 [87], allowing a quantitatively accurate determination of defect level positions in the gap. HSE06 does not reproduce the band gap of, e.g., β-Ga_2O_3, however, it has been shown that [44] simultaneously tuning α and μ to reproduce the band gap and fulfill the gKT leads to defect levels in good agreement with experimental observations.

The standard HSE06 does not fulfill the two criteria mentioned above for our IB host material $CuGaS_2$ either. In previous work, either the mixing parameter ($\alpha = 0.3$) [83] or the screening parameter ($\mu = 0.13$) [42] was tuned to improve the band gap, but both fail to satisfy the gKT as can be seen from Table I. Therefore, we have searched for an optimized HSE(α,μ) functional, tuning the parameters to meet both criteria simultaneously. The experimental optical band gap of $CuGaS_2$ at RT is 2.43 eV [88,89], which increases to about 2.53 eV as the temperature decreases to 2 K [90–92]. Due to excitonic effects and electron-phonon interactions, the low-temperature optical gap is always somewhat smaller than the quasiparticle band gap obtained in a theoretical calculation. The latter can only be compared to low-temperature photoelectron spectroscopy data but, unfortunately, those are not available for $CuGaS_2$. However, a first-principles many-body calculation [self-consistent Coulomb hole and screened exchange G_0W_0 (scCOHSEX + G_0W_0)] [28] resulted in 2.65 eV, in compliance with the expectation. Considering the uncertainties of the optimization (limited supercell size, k-point set, and fixed lattice parameters during parameter optimization), we have chosen 2.6 eV as the target gap value. Table I shows the band gap of the perfect 128-atom supercell and the KS level of the highest occupied molecular orbital (HOMO) for the neutral and of the lowest unoccupied molecular orbital (LUMO) for the positive charged state of Sn_{Ga} with respect to the CB minimum (CBM) (ΔKS). ΔE_{SCF} is the electron-removal energy obtained from the difference of self-consistent total

TABLE II. Calculated band gap (in eV), lattice parameters a and c [in angstroms (Å)], volume (in Å^3), c/a ratio, the anion displacement parameter u (in Å), and the bulk modulus (in GPa), calculated with different functionals, in comparison with experiment.

$CuGaS_2$	E_g	a	c	Volume	c/a	u	B_0
Expt. [51,93,94]	2.53[a]	5.351	10.478	300.03	1.959	0.259	94–96
GGA [95]	0.62	5.388	10.668	309.7	1.980	0.247	77.6
HSE(0.25,0.13) [95]	2.44	5.366	10.555	303.92	1.967	0.253	79.3
HSE(0.26,0.08)	2.61	5.359	10.531	302.42	1.965	0.255	81.64

[a]Optical gap at 2 K.

energies between the neutral and the positive charge states at fixed geometry, referenced also to the CBM. According to the gKT, the three values should be equal. This is achieved approximately with the combination of $\alpha = 0.26$ and $\mu = 0.08$, resulting in a band gap of 2.55 eV for the 128-atom supercell. We also have checked the fulfillment of the gKT on the divacancy of ($V_S + V_{Cu}$) in the 1− charge state and found ΔKS_{HOMO} (N), ΔE_{SCF} (eV), and ΔKS_{LUMO} ($N - 1$) to be within 0.1 eV.

Having obtained the ideal HSE(α,μ) functional, we have used it to optimize the geometry of the primitive cell and calculate the band structure. The band gap, lattice parameters, and bulk modulus are listed in Table II, in comparison to other results. As can be seen, the optimized hybrid functional provides for improvement in all the parameters.

Finally we note that screening can be both orbital and direction dependent, which cannot be reproduced by the simple approach of a HSE(α,μ) functional. Therefore, the reproduction of the band gap in the zone center alone does not guarantee the accurate description of the CBM and the VBM over the entire Brillouin zone, which is a necessity for predicting accurate defect levels [44,45]. Comparison of the band structure obtained by the optimized hybrid functional to the scCOHSEX + G_0W_0 results of Ref. [28] has assured us, however, that the dispersion and the band gap at the k-points T, Γ, and N are in good agreement.

C. Tests of HSE(0.26,0.08) on $CuGaSe_2$

Since we were not able to find experimental results on deep defect levels in $CuGaS_2$, to assess our optimized HSE(0.26,0.08) functional, we tested it on the known defects in $CuGaSe_2$. Because the parameters of an optimal HSE(α,μ) functional are material dependent, we checked first whether the parameters found for $CuGaS_2$ are transferable to $CuGaSe_2$. Using HSE(0.26,0.08), the gKT is satisfied within 0.03 eV also in the latter material, and the band gap of 1.76 eV also appears to be appropriate, considering the experimental optical gap of 1.73 eV at 77 K [96,97]. Therefore, HSE(0.26,0.08) also works well for $CuGaSe_2$ [98], which is a much more widely investigated material with defect data readily available in the literature. In the following, we will first check the accuracy of the optimized hybrid by calculating the observed PL related to the Ga_{Cu} antisite defect [99]. Then we will go on to show what difference the optimized hybrid makes with respect to earlier calculations on the antisite defects Ga_{Cu} and Cu_{Ga} in $CuGaSe_2$ [37–39,42] and to Sn_{Ga} in $CuGaS_2$.

A PL study on $CuGaSe_2$ has found two bands at 1.10 and 1.24 eV [99], which have been assigned to recombination between a common shallow acceptor and two deep donor states. For the latter the Ga_{Cu} antisite and its complex with a copper vacancy have been suggested. The shallow acceptor level within 100 meV of the VBM was not identified. Assuming that, within the limits posed by the supercell approach, the shallow acceptor would be no more localized than a hole on the VBM of our 128-atom supercell, we have calculated the energy of recombination between a neutral Ga_{Cu} defect and a hole in the VBM as depicted in Fig. 2. First we have relaxed the system with a hole at the VBM then fixed the final geometry and recalculated the energy with the hole now on the defect level. The difference in the two energies supplies the PL energy. Considering the delocalization of the hole in the initial state, in this calculation we have used a larger $2 \times 2 \times 1$ k-point set. After proper corrections (for charge as well as for band-filling effects [100]), we obtain 1.30 eV. Assuming the acceptor level to be 100 meV above the VB, our estimation of the PL energy is 1.20 eV, which is well within the range of the observed values. Apparently, the optimized hybrid functional can reproduce defect-related energies in $CuGaSe_2$ with an accuracy of ±0.1 eV.

In order to evaluate the effect of the optimal HSE(0.26,0.08), we compare our results on Ga_{Cu} and Cu_{Ga} in $CuGaSe_2$ and on Sn_{Ga} in $CuGaS_2$ to those obtained by the HSE(0.25,0.13) functional used by Pohl and Albe [42]. Table III shows the gap levels with respect to the band edges, i.e., the vertical electronic transitions, calculated under identical conditions in columns 2 and 3. The increase in the HF fraction and the decrease in the screening parameter both have a localizing effect, which make the one-electron levels deeper by about 0.2 eV. Table III also compares the results obtained from the 128-atom Γ-point calculation with the values published for a 216-atom supercell with a $2 \times 2 \times 2$ MP set. The difference is within 0.1 eV as mentioned earlier.

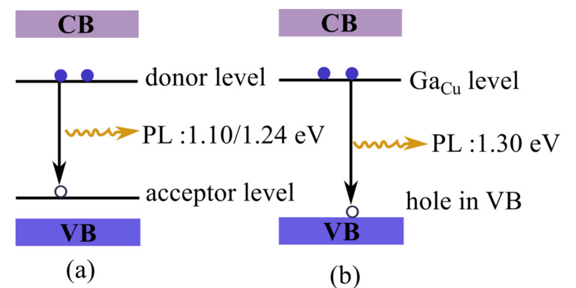

FIG. 2. Schematic of the PL related to the Ga_{Cu} defect in $CuGaSe_2$. (a) Experimental results in Ref. [99]. (b) The present calculation.

TABLE III. Gap levels of the neutral defects with respect to the band edges (in eV), calculated with the optimized hybrid functional and with the one fitted to the band gap only in Ref. [42]. (Acceptor/donor levels are referenced to the VBM/CBM.)

$CuGaSe_2$	HSE(0.26,0.08) 128 atoms, Γ approximation	HSE(0.25,0.13) 128 atoms, Γ approximation	HSE(0.25,0.13) [42] 216 atoms, 2 × 2 × 2
Cu_{Ga}	+0.60	+0.45	+0.36
Ga_{Cu}	−0.78	−0.49	−0.53
$CuGaS_2$			
Sn_{Ga}	−1.56	−1.37	Not available

A similar comparison is shown in Table IV for the adiabatic charge transition levels. Looking first at the results obtained under identical conditions (in the 128-atom cell using the Γ approximation and ε_∞ for the charge correction), the adiabatic levels also are deeper with the optimized functional, although the difference is smaller than that for the vertical transitions. In order to evaluate size effects, we also compare to the values published in Ref. [42]. For this purpose, we have recalculated our results using ε_0 in the charge correction as in Ref. [42] (see column 4). The differences between the 128-atom Γ-point and the 216-atom 2 × 2 × 2 calculations (column 5) are around 0.1 eV.

For comparison to experiment, we have added the difference between columns 5 and 4 to the results of the optimized hybrid functional in column 2 of Table Table IV, resulting in an activation energy of 0.35 eV for the acceptorlike (electron trap) Cu_{Ga} (0/−1), and 0.38 eV for the donorlike (hole trap) Ga_{Cu} (+/0) in $CuGaSe_2$. Experimentally, a number of electron and hole traps are observed in the energy range of 0.10–0.68 and 0.13–0.80 eV, respectively [101–103]. Specifically, in copper-rich material, two acceptorlike traps have been found with activation energies between 0.186–0.240 and 0.375–0.390 eV [104]. Cu_{Ga} is a low formation-energy defect in copper-rich material [42], and our (size-corrected) result for the activation energy 0.35 eV seems to be quite close to that of the deeper trap. In contrast to the copper-rich case where the free-carrier density is about 10^{17} cm^{-3}, gallium-rich samples show carrier densities around 10^{12} cm^{-3} (unless sodium contamination is present) [104]. This means that the unintentional *p*-type doping is strongly passivated and the Fermi level is pinned at 0.381 eV above the VB [104]. Now in gallium-rich samples the donorlike Ga_{Cu} is expected to be dominant [42]. Its (size-corrected) (+/0) transition level is at 1.76–0.38 = 1.38 eV above the VBM (where $E_g = 1.76$ eV), therefore, it can passivate the unintentional acceptors, pinning the Fermi level below midgap. We may assume V_{Cu} vacancies to be the majority acceptors in copper-poor samples. Solving Eqs. (1) and (2) using the data of Ref. [42] and considering only single ionization of both V_{Cu} and Ga_{Cu}, we estimate the Fermi level to be pinned at about 0.5 eV above the VBM, which compares favorably with the experimental 0.4 eV.

III. RESULTS

As mentioned in the Introduction, the idea of a deep level impurity intermediate band in bulk solar cell materials has not so far fulfilled the expectations for an efficiency increase. To shed light on possible reasons, we now apply the optimized HSE functional to study the Sn_{Ga} impurity in $CuGaS_2$ as a typical example.

The Sn atoms on Ga sites introduce one extra electron each, which are expected to be in a half-filled defect band in the gap for high-Sn_{Ga} concentration. In fact, a spin-polarized calculation results in an occupied and an empty gap level with quite different energies upon introduction of a single Sn_{Ga}^0 dopant into the 128-atom supercell (see Table V). This corresponds to a concentration of $\sim 4 \times 10^{20}$ cm^{-3}, so, based on the 1.25-eV difference (at Γ), the formation of a full band and of an empty band is expected without overlap even for higher concentrations. (Note, that the even-electron systems Sn_{Ga}^+ and Sn_{Ga}^- have a closed-shell electron configuration with the two holes or the two electrons, respectively, having the same energy.) We would like to point out that the level positions shown in Table V correspond to the vertical charge transition levels due to the fulfillment of the gKT. Therefore, the values given for the neutral charge states indicate the possibility for a VB-to-defect transition of (2.61–0.31) = 2.30 eV (where $E_g = 2.61$ eV) and a defect-to-CB transition of 1.56 eV. Such transitions could, indeed, increase the efficiency of utilizing sunlight.

With an occupied state and an empty state in the gap, both the positive and the negative charge states of Sn_{Ga} can be stable. We have calculated the (0/−) and the (+/0) adiabatic charge transition levels. The results show (see Table VI) that

TABLE IV. Adiabatic charge transition levels (in eV), calculated with the optimized hybrid and with the one fitted to the band gap only in Ref. [42]. (Acceptor/donor levels are referenced to the VBM/CBM.)

$CuGaSe_2$	HSE(0.26,0.08) 128 atoms, Γ approximation correction with ε_∞	HSE(0.25,0.13) 128 atoms, Γ approximation correction. with ε_∞	HSE(0.25,0.13) 128 atoms, Γ approximation correction with ε_0	HSE(0.25,0.13) 216 atoms, 2 × 2 × 2 Ref. [42]
Cu_{Ga} (0/−)	+0.47	+0.37	+0.32	+0.20
Ga_{Cu} (+/0)	−0.48	−0.44	−0.45	−0.35
$CuGaS_2$				
Sn_{Ga} (+/0)	−1.09	−1.02	−0.98	Not available

TABLE V. Single-particle defect levels (at the Γ point) introduced by Sn_{Ga} and Cu_{Ga} into $CuGaS_2$ in the spin channels α and β with respect to the band edges (in eV). N.B.: These values correspond to vertical charge transition levels due to the fulfillment of the gKT. For more explanations, see the text.

$CuGaS_2$	Charge state	ε_α	Occupancy	ε_β	Occupancy
	+	$E_C - 0.71$	0	$E_C - 0.71$	0
Sn_{Ga}	0	$E_C - 1.56$	1	$E_C - 0.31$	0
	−	$E_C - 1.18$	1	$E_C - 1.18$	1
	0	$E_V + 0.78$	0	$E_V + 0.78$	0
Cu_{Ga}	−	Resonance	1	$E_V + 1.50$	0
	2−	Resonance	1	Resonance	1

Sn^0_{Ga} is stable with the Fermi-level positions between 0.74 and 1.09 eV below the CBM, but the charged states also have a substantial stability range. This means that Sn^0_{Ga} is an amphoteric trap, capable of capturing both free holes from the valence band and free electrons from the conduction band. Therefore, it is expected that the excited electron-hole pairs will recombine quickly at this defect. We cannot calculate the nonradiative recombination rates here, but we can estimate the relative likelihood of the radiation-induced electronic transition $Sn^0_{Ga} \rightarrow$ CB and the radiative recombination CB $\rightarrow Sn^0_{Ga}$, based on calculated dielectric functions.

To do that, we assume that the probability of the CB $\rightarrow Sn^0_{Ga}$ transition is the same as that of the reverse transition $Sn^-_{Ga} \rightarrow$ CB. Similarly, we can estimate the relative likelihood of the VB $\rightarrow Sn^0_{Ga}$ and $Sn^0_{Ga} \rightarrow$ VB optical transitions assuming the probability of the latter to be equal with the reverse transition VB $\rightarrow Sn^+_{Ga}$. The imaginary part of the calculated dielectric function depends on the transition probabilities, so for Sn^0_{Ga}, Sn^-_{Ga}, and Sn^+_{Ga}, it is shown in Fig. 3 in the sub-band-gap region of $CuGaS_2$. The peaks around $E_V + 2.3$ eV correspond to transitions between the VB and the defect, whereas those around 1.6 eV correspond to transitions between the defect and the CB. The integrated areas below the peaks have an approximate 2:1 ratio between $Sn^-_{Ga} \rightarrow$ CB and $Sn^0_{Ga} \rightarrow$ CB on one hand and between VB $\rightarrow Sn^+_{Ga}$ and VB $\rightarrow Sn^0_{Ga}$ on the other hand. Considering the number of available electrons and holes, respectively, this means that the transition probabilities are just about equal. In other words, the likelihood of optical excitation and radiative recombination is equal, which indicates a short lifetime of the excited carriers. This means that, even in case of substantial absorption at the desired wavelengths, the actual current still remains low.

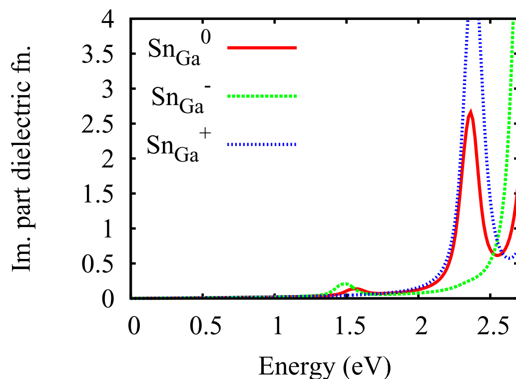

FIG. 3. Imaginary part of the dielectric function Im{$\varepsilon(E)$} in the sub-band-gap region for Sn^+_{Ga}, Sn^0_{Ga}, and Sn^-_{Ga} in $CuGaS_2$.

TABLE VI. Adiabatic charge transitional levels of Sn_{Ga} and Cu_{Ga} in $CuGaS_2$. All in eV.

$CuGaS_2$		Adiabatic charge transition
Sn_{Ga}	(+/0)	$E_C - 1.09$
	(0/−)	$E_C - 0.74$
Cu_{Ga}	(0/−)	$E_V + 0.54$
	(−/2−)	$E_V + 1.46$

When considering the effect of a dopant, passivation mechanisms by intrinsic defects should be taken into account [105,106]. The incorporation of Sn onto a Ga site requires gallium-poor conditions where Sn_{Ga} has to compete with Cu_{Ga} antisites, which are low formation-energy acceptors [107], so we consider Cu_{Ga} as the defect that may passivate the Sn_{Ga} donor. As shown in Table V, Cu_{Ga} has an empty level 0.78 eV above the VBM, i.e., it is a deep double acceptor which can act as an electron trap. (We note that, upon accepting electrons, the occupied states shift down into the VB, whereas relatively delocalized states appear close but above the VB edge. We believe these to be an artifact of the much too small supercell, whereas the defect-related occupied states are resonant with the VB.)

Table VI shows the adiabatic charge transition levels of the Cu_{Ga} acceptor. The formation energies of Sn_{Ga} and Cu_{Ga} in $CuGaS_2$, calculated according to Eq. (1), are plotted as a function of the Fermi energy in Fig. 4. In a p-type sample (Fermi level in the lower half of the gap), Sn_{Ga} is energetically preferred above Cu_{Ga} and is charged positively. An increasing concentration of the Sn_{Ga} donor would shift the Fermi level up but, as a consequence, Cu_{Ga} becomes negatively charged,

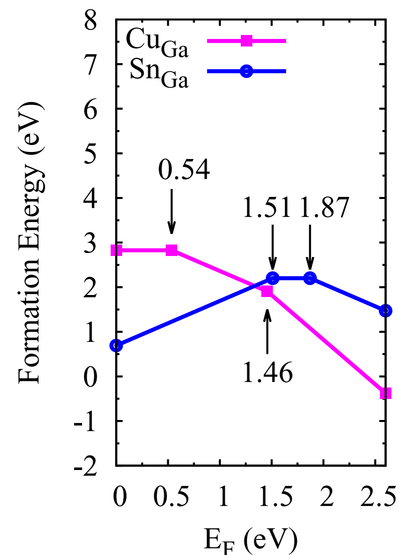

FIG. 4. Defect formation energy in $CuGaS_2$. The arrows show the adiabatic charge transition levels.

TABLE VII. Formation energy (in eV) of charged defects, referred to the valence-band maximum, assuming the metallic chemical potentials of Sn, Cu, and Ga to be that of the metallic states.

Defect	q	$E_{\text{form}}^{i,q} + qE_F$
	+	0.69
Sn_{Ga}	0	2.20
	−	4.07
	0	2.83
Cu_{Ga}	−	3.36
	2−	4.82

and its formation energy starts to diminish. This means that increasing the Sn_{Ga} concentration leads to an increase in the Cu_{Ga} concentration as well. The reason is that Cu_{Ga} becomes negatively ionized at the expense of the Sn_{Ga} donors, so they become mutually passivated. Energy is gained by transferring electrons from Sn_{Ga} to Cu_{Ga} until the formation-energy curves cross. The self-consistent solution of the charge neutrality equations, Eqs. (1) and (2), with the calculated formation energy values shown in Table VII, results in a Fermi level pinned at 1.4 eV above the VBM, close to the crossing point of the two curves in Fig. 4. At this Fermi-level position Cu_{Ga} is in the negative charge state (singly and doubly in about equal concentrations), whereas Sn_{Ga} is dominantly in the positive charge state. In other words, Sn_{Ga} donors induce the spontaneous formation of Cu_{Ga} acceptors, which fully passivate them.

In this circumstance, as can be seen in Table V, Sn_{Ga}^{+} and $Cu_{Ga}^{-,2-}$ introduce empty levels deep in the gap at 2.61–0.71 = 1.90 eV and at 1.50 eV above the VBM, respectively (E_g = 2.61 eV) but occupied levels only very near to the VB at most. These levels make VB-to-defect excitations possible but not the defect-to-CB excitations. Such an effect could also explain the observation of Ref. [33] in $CuInS_2$:Sn_{In}. For $CuGaS_2$:Sn_{Ga} the level positions mean that only red light can additionally be utilized due to the doping but not green light as expected without passivation. Accordingly, the efficiency increase is smaller than expected.

IV. SUMMARY

We have investigated the Sn_{Ga} defect in $CuGaS_2$, which has been proposed to form a half-filled intermediate band in the gap, allowing for the utilization of red and green light in solar cells. We have used an optimized HSE(α,μ)-type hybrid functional which reproduces the low-temperature band gaps of $CuGaS_2$ and $CuGaSe_2$ and fulfills the generalized Koopmans' theorem with $\alpha = 0.26$ and $\mu = 0.08$. Such hybrids can successfully mimic the exact DFT functional if the screening in the material is not direction/orbital dependent, which is the case here. Indeed, the optimized functional reproduces the observed PL related to the Ga_{Cu} antisite in $CuGaSe_2$ quite accurately and predicts the charge transition level of the Cu_{Ga} acceptor very close to that of a well-known acceptorlike trap observed in copper-rich material. Applying this hybrid functional in $CuGaS_2$, we have found that Sn_{Ga} is an amphoteric trap. We show that the radiative recombination has the same likelihood as that of the radiation-induced excitation, which limits the carrier lifetime, i.e., the achievable current. In addition, we have found that Sn_{Ga} doping leads to the spontaneous formation of Cu_{Ga} acceptors, and the two defects passivate each other, pinning the Fermi level at $E_V + 1.4$ eV. The ionized Sn_{Ga}^{+} and $Cu_{Ga}^{-,2-}$ defects make VB-to-defect transitions possible upon excitation by red light but no defect-to-CB excitation utilizing the yellow-green part of the spectrum as expected.

Beyond the specific problem of Sn_{Ga} in $CuGaS_2$, investigated here, the effect of self-induced passivation appears to be relevant in all systems with multiple cations or anions. For example, in a $C1C2A_2$ compound, substitution of cation C2 by a donor D requires C2-poor conditions. However, in that case, C1 and D will compete for the C2 sites. If the valence of C1 is less than that of C2, the resulting anitisite $C1_{C2}$ will be an acceptor, and the energy, gained by transferring electrons from the donors to the acceptors, will favor simultaneous incorporation of the two, i.e., passivation of the donor. Therefore, we believe that our findings are generally relevant for IB dopants in CIGS material and, from the perspective of defect physics, enable to explain some of the experimental problems seen so far, such as insignificant absorption enhancement, no photocurrent, and efficiency enhancement. More defect physics studies should be performed to have a better estimation of the performance of such kinds of IB solar cells.

ACKNOWLEDGMENTS

We thank S. Siebentritt for useful discussions. This work has been supported by the special Funds for Major State Basic Research Project of China Project No. (973) under Grant No. 2012CB933702 and the NSFC under Grants No. 11204310 and No. 11534012. M.H. was supported by the China Scholarship Council. Support of the Supercomputer Center of Northern Germany (HLRN Grant No. hbc00017) is acknowledged.

[1] A. Luque and A. Martí, Phys. Rev. Lett. **78**, 5014 (1997).
[2] A. Luque, A. Martí, and C. Stanley, Nat. Photonics **6**, 146152 (2012).
[3] B. Marsen, S. Klemz, T. Unold, and H.-W. Schock, Prog. Photovoltaics **20**, 625 (2012).
[4] A. Martí, D. F. Marrón, and A. Luque, J. Appl. Phys. **103**, 073706 (2008).
[5] W. Shockley and H. J. Queisser, J. Appl. Phys. **32**, 510 (1961).
[6] A. Martí, E. Antoltín, C. R. Stanley, C. D. Farmer, N. López, P. Díaz, P. G. Linares, and A. Luque, Phys. Rev. Lett. **97**, 247701 (2006).
[7] C. G. Bailey, D. V. Forbes, R. P. Raffaelle, and S. M. Hubbard, Appl. Phys. Lett. **98**, 163105 (2011).
[8] S. Dhomkar, U. Manna, L. Peng, R. Moug, I. C. Noyan, M. C. Tamargo, and I. L. Kuskovsky, Sol. Energy Mater. Sol. Cells **117**, 604–609 (2013).

[9] S. Tomić, Phys. Rev. B **82**, 195321 (2010).
[10] S. M. Hubbard, C. D. Cress, C. G. Bailey, R. P. Raffaelle, S. G. Bailey, and D. M. Wilt, Appl. Phys. Lett. **92**, 123512 (2008).
[11] R. Oshima, A. Takata, and Y. Okada, Appl. Phys. Lett. **93**, 083111 (2008).
[12] W. Wang, A. S. Lin, and J. D. Phillips, Appl. Phys. Lett. **95**, 011103 (2009).
[13] N. Ahsan, N. Miyashita, M. M. Islam, K. M. Yu, and W. Walukiewicz, and Y. Okada, J. Appl. Phys. **100**, 172111 (2012).
[14] T. Tanaka, M. Miyabara, Y. Nagao, K. Saito, Q. Guo, M. Nishio, K. M. Yu, and W. Walukiewicz, Appl. Phys. Lett. **102**, 052111 (2013).
[15] S. Kurtz, J. F. Geisz, B. M. Keyes, W. K. Metzger, D. J. Friedman, J. M. Olson, A. J. Ptak, R. R. King, and N. H. Karam, Appl. Phys. Lett. **82**, 2634 (2003).
[16] W. Shan, W. Walukiewicz, J. W. Ager, III, E. E. Haller, J. F. Geisz, D. J. Friedman, J. M. Olson, and S. R. Kurtz, Phys. Rev. Lett **82**, 1221 (1999).
[17] A. Luque, A. Martí, E. Antolín, and C. Tablero, Physica B **382**, 320 (2006).
[18] P. Palacios, I. Aguilera, K. Sánchez, J. C. Conesa, and P. Wahnón, Phys. Rev. Lett. **101**, 046403 (2008).
[19] I. Aguilera, P. Palacios, and P. Wahnón, Thin Solid Films **516**, 7055 (2008).
[20] M. Han, X. Zhang, and Z. Zeng, RSC Adv. **4**, 62380 (2014).
[21] I. Aguilera, P. Palacios, and P. Wahnón, Sol. Energy Mater. Sol. Cells **94**, 1903 (2010).
[22] P. Palacios, K. Sánche, J. C. Conesa, and P. Wahnón, Phys. Status Solidi A **203**, 1395 (2006).
[23] P. Palacios, K. Sánche, J. C. Conesa, J. J. Fernández, and P. Wahnón, Thin Solid Films **515**, 6280 (2007).
[24] C. Tablero, Thin Solid Films **519**, 1435 (2010).
[25] C. Tablero, J. Appl. Phys. **106**, 073718 (2009).
[26] P. Jackson, D. Hariskos, E. Lotter, S. Paetel, R. Wuerz, R. Menner, W. Wischmann, and M. Powalla, Prog. Photovoltaics **19**, 894 (2011).
[27] A. Chirilá, P. Reinhard, F. Pianezzi, P. Bloesch, A. R. Uhl, C. Fella, L. Kranz, D. Keller, C. Gretener, H. Hagendorfer, D. Jaeger, R. Erni, S. Nishiwaki, S. Buecheler, and A. N. Tiwari, Nature Mater. **12**, 1107 (2013).
[28] I. Aguilera, J. Vidal, P. Wahnón, L. Reining, and S. Botti, Phys. Rev. B **84**, 085145 (2011).
[29] J. L. Shay, J. H. Wernick, and B. R. Pamplin, *Ternary Chalcopyrite Semiconductors: Growth Electronic Properties and Applications*, International Series in the Science of the Solid State Vol. 7 (Pergamon, Oxford, 1975), p. 110.
[30] X. Lv, S. Yang, M. Li, H. Li, J. Yi, M. Wang, and J. Zhong, Solar Energy **103**, 480 (2014).
[31] P. Chen, M. Qin, H. Chen, C. Yang, Y. Wang, and F. Huang, Phys. Status Solidi A **210**, 1098 (2013).
[32] T. Teranishi, K. Sato, and K. Knodo, J. Phys. Soc. Jpn. **36**, 1618 (1974).
[33] C. Yang, M. Qin, Y. Wang, D. Wan, F. Huang, and J. Lin, Sci. Rep. **3**, 1286 (2013).
[34] S. Song, Y. Wang, X. Yuan, W. Yao, and W. Jing, Mater. Lett. **148**, 41 (2015).
[35] Note, however, that for $CuInS_2:Sn_{In}$, photoluminescence was observed only due to transitions from the IB to the VB but none due to transitions from the CB to the IB.
[36] C. Tablero and D. F. Márron, J. Phys. Chem. C **114**, 2756 (2010).
[37] S.-H. Wei, S. B. Zhang, and A. Zunger, Appl. Phys. Lett. **72**, 3199 (1998).
[38] S. B. Zhang, S.-H. Wei, A. Zunger, and H. Katayama-Yoshida, Phys. Rev. B **57**, 9642 (1998).
[39] S.-H. Wei and S. B. Zhang, J. Phys. Chem. Solids **66**, 1994 (2005).
[40] J. Heyd, G. E. Scuseria, and M. Ernzerhof, J. Chem. Phys. **118**, 8207 (2003).
[41] J. Heyd, G. E. Scuseria, and M. Ernzerhof, J. Chem. Phys. **124**, 219906 (2006).
[42] J. Pohl and K. Albe, Phys. Rev. B **87**, 245203 (2013).
[43] P. Deák, *in Computational Materials Science*, edited by R. Catlow and E. Kotomin, NATO Science Series III, Vol. 187 (IOS, Amsterdam 2003), p. 255.
[44] P. Deák, Q. Duy Ho, F. Seemann, B. Aradi, M. Lorke, and T. Frauenheim, Phys. Rev. B **95**, 075208 (2017).
[45] P. Deák, Physica B (2017), doi:10.1016/j.physb.2017.06.024.
[46] G. Kresse and J. Hafner, Phys. Rev. B **49**, 14251 (1994).
[47] G. Kresse and J. Furthmüller, Comput. Mater. Sci. **6**, 15 (1996).
[48] G. Kresse and J. Furthmüller, Phys. Rev. B **54**, 11169 (1996).
[49] G. Kresse and D. Joubert, Phys. Rev. B **59**, 1758 (1999).
[50] P. E. Blöchl, Phys. Rev. B **50**, 17953 (1994).
[51] S. C. Abrahams and J. L. Bernstein, J. Chem. Phys. **59**, 5415 (1973).
[52] H. J. Monkhorst and J. D. Pack, Phys. Rev. B **13**, 5188 (1976).
[53] F. D. Murnaghan, Proc. Natl. Acad. Sci. U.S.A. **30**, 244 (1944).
[54] F. Birch, Phys. Rev. **71**, 809 (1947).
[55] S. B. Zhang and J. E. Northrup, Phys. Rev. Lett. **67**, 2339 (1991).
[56] A. Zunger, *in Solid State Physics*, edited by H. Ehrenreich and D. Turnbull Vol. 39 (Academic, New York, 1986), p. 275.
[57] Y. Zhang, J. R. G. Evans, and S. Yang, J. Chem. Eng. Data. **56**, 328 (2011).
[58] H.-P. Komsa, T. T. Rantala, and A. Pasquarello, Phys. Rev. B **86**, 045112 (2012).
[59] C. Freysoldt, J. Neugebauer, and C. G. Van de Walle, Phys. Rev. Lett. **102**, 016402 (2009).
[60] W. Chen and A. Pasquarello, Phys. Rev. B **88**, 115104 (2013).
[61] J. Baars and W. H. Koschel, Solid State Commun. **11**, 1513 (1972).
[62] R. Márquez and C. Rincón, Phys. Status Solidi B **191**, 115 (1995).
[63] C. Parlak and R. Eryiğit, Phys. Rev. B **73**, 245217 (2006).
[64] See Supplemental Material at http://link.aps.org/supplemental/10.1103/PhysRevB.96.165204 for the raw energy results together with the applied corrections.
[65] P. Deák, B. Aradi, M. Kaviani, T. Frauenheim, and A. Gali, Phys. Rev. B **89**, 075203 (2014).
[66] P. W. Yu, D. L. Downing, and Y. S. Park, J. Appl. Phys. **45**, 5283 (1974).
[67] N. N. Syrbu, I. M. Tiginyanu, L. L. Nemerenco, V. V. Ursaki, V. E. Tezlevan, and V. V. Zalamai, J. Phys. Chem. Solids **66**, 1974 (2005).
[68] P. Prabukanthan and R. Dhanasekaran, Cryst. Growth Des. **7**, 618 (2007).
[69] J. P. Perdew, A. Ruzsinszky, G. I. Csonka, O. A. Vydrov, G. E. Scuseria, V. N. Staroverov, and J. Tao, Phys. Rev. A **76**, 040501(R) (2007).

[70] P. Mori-Sánchez, A. J. Cohen, and W. Yang, Phys. Rev. Lett. **100**, 146401 (2008).
[71] J. P. Perdew, R. G. Parr, M. Levy, and J. L. Balduz, Phys. Rev. Lett. **49**, 1691 (1982).
[72] S. Lany and A. Zunger, Phys. Rev. B **80**, 085202 (2009).
[73] C.-O. Almbladh and U. von Barth, Phys. Rev. B **31**, 3231 (1985).
[74] W. R. L. Lambrecht, Phys. Status Solidi B **248**, 1547 (2011).
[75] C. Freysoldt, B. Grabowski, T. Hickel, J. Neugebauer, G. Kresse, A. Janotti, and C. G. V. de Walle, Rev. Mod. Phys. **86**, 253 (2014).
[76] S. J. Clark and J. Robertson, Phys. Rev. B **82**, 085208 (2010).
[77] X. Zheng, A. J. Cohen, P. Mori-Sánchez, X. Hu, and W. Yang, Phys. Rev. Lett. **107**, 026403 (2011).
[78] T. M. Henderson, J. Paier, and G. E. Scuseria, Phys. Status Solidi B **248**, 767 (2011).
[79] J. P. Perdew, K. Burke, and M. Ernzerhof, Phys. Rev. Lett. **77**, 3865 (1996).
[80] J. Paier, M. Marsman, K. Hummer, G. Kresse, I. C. Gerber, and J. G. Ángyán, J. Chem. Phys. **124**, 154709 (2006).
[81] M. Marsman, J. Paier, A. Stroppa, and G. Kresse, J. Phys.: Condens. Matter **20**, 064201 (2008).
[82] W. Gao, T. C. T. Abtew, Y. Y. Sun, S. B. Zhang, and P. Zhang, arXiv:1504.06259.
[83] M. Han, X. Zhang, and Z. Zeng, RSC Adv. **6**, 110511 (2016).
[84] X. Zhang, M. Han, and Z. Zeng, J. Mater. Chem. A **5**, 6606 (2017).
[85] P. Deák, B. Aradi, T. Frauenheim, E. Janzén, and A. Gali, Phys. Rev. B **81**, 153203 (2010).
[86] P. Deák, A. Gali, B. Aradi, and T. Frauenheim, Phys. Status Solidi B **248**, 790 (2011).
[87] P. Deák, B. Aradi, and T. Frauenheim, Phys. Rev. B **83**, 155207 (2011).
[88] L. Shay and J. Wernick, *Ternary Chalcopyrite Semiconductors* (Pergamon, Oxford, 1975).
[89] M. I. Alonso, K. Wakita, J. Pascual, M. Garriga, and N. Yamamoto, Phys. Rev. B **63**, 075203 (2001).
[90] B. Tell, J. L. Shay, and H. M. Kasper, Phys. Rev. B **4**, 2463 (1971).
[91] B. Tell and H. M. Kasper, Phys. Rev. B **7**, 740 (1973).
[92] C. Bellabarba, J. González, and C. Rincón, Phys. Rev. B **53**, 7792 (1996).
[93] M. Bettini and W. Holzapfel, Solid State Commun. **16**, 27 (1975).
[94] A. Werner, H. D. Hochheimer, and A. Jayaraman, Phys. Rev. B **23**, 3836 (1981).
[95] J. Pohl and K. Albe, J. Appl. Phys. **108**, 023509 (2010).
[96] M. P. Vecchi, J. Ramos, and W. Giriat, Solid-State Electronics **21**, 1609 (1978).
[97] B. Tell and P. Bridenbaugh, Phys. Rev. B **12**, 3330 (1975).
[98] N.B.: The same is not true for $CuInS_2$.
[99] C. Spindler, D. Regesch, and S. Siebentritt, Appl. Phys. Lett. **109**, 032105 (2016).
[100] S. Lany and A. Zunger, Phys. Rev. B **78**, 235104 (2008).
[101] A. Krysztopa, M. Igalson, Y. Aida, J. K. Larsen, L. Gütay, and S. Siebentritt, J. Appl. Phys. **110**, 103711 (2011).
[102] A. Krysztopa, M. Igalson, J. K. Larsen, Y. Aida, L. Gütay, and S. Siebentritt, J. Phys. D.: Appl. Phys. **45**, 335101 (2012).
[103] V. Mertens, J. Parisi, and R. Reineke-Koch, J. Appl. Phys. **101**, 104507 (2007).
[104] A. Jasenek, U. Rau, and H. W. Schock, J. Appl. Phys. **87**, 594 (2000).
[105] S. Lany, J. Osorio-Guillén, and A. Zunger, Phys. Rev. B **75**, 241203(R) (2007).
[106] Y. Yan and S.-H. Wei, Phys. Status Solidi B **245**, 641 (2008).
[107] C. L. Bailey, L. Liborio, G. Mallia, S. Tomić, and N. M. Harrison, Phys. Rev. B **81**, 205214 (2010).